Journal of Computational and Applied Mechanics, Vol. 4., No. 2., (2003), pp. 159–173

INVESTIGATION OF THE DEFORMATION OF A MULTILAYERED PIEZOELECTRIC SEMIRING

Pál Zoltán Kovács
Department of Mechanics, University of Miskolc
3515 Miskolc-Egyetemváros A/4, Hungary
mechanik@uni-miskolc.hu

István Páczelt
Department of Mechanics, University of Miskolc
3515 Miskolc-Egyetemváros A/4, Hungary
mechpacz@uni-miskolc.hu

[Received: January 30, 2002]

Abstract. A semicircular planar prismatic beam is subjected to bending moments resulting from piezoelectric actuator devices bonded to the parallel surfaces of the beam. The bending and torsional deformations are investigated with the Finite Element Method (FEM) and the closed-form solution of the linear theory of 3D curved beams, respectively. The geometry of curved element segments is mapped exactly by using the blending function method and with the Legendre polynomials (isoparametric functions). The aim of the study is to demonstrate that a planar curved beam under piezoelectric load deflects and twists additionally.

Mathematical Subject Classification: 74E30,74F99,74K10
Keywords: piezoelectric actuator, blending functions, bending rigidity, FEM

1. Introduction

This study presents an investigation of a semicircular prismatic cantilever beam, the centerline of which is a planar curvilinear arc. Its parallel surfaces are covered by PIC151 piezoelectric patches (Figure 1).

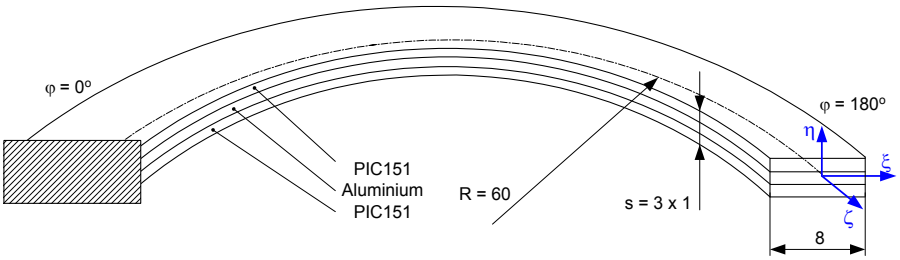

Figure 1. Composite semiring

Particularly, the linear theory of space curved beams is used and the results are compared to those obtained by the FEM. The inverse piezoelectric effect is realised by generating an electric potential difference between the piezoelectric surfaces perpendicular to the η-direction, which is the direction of its natural polarization. The longitudinal stresses in the actuators result in the contraction and the expansion of the external fibres of the basic aluminium beam, respectively. The effect generates a bending moment along the beam, which causes the deflection along the centerline and the angular rotations of the cross-sections. The aim of the study is to determine these deformations by using the closed form solution and to compare them to the approximate solution. The procedure is assumed to be quasi-static, the displacements and strains are considered to be small. The layers are bonded to each other through a glue layer with zero thickness. The aluminium beam is assumed to be isotropic, the piezoelectric material based on PIC151 is orthotropic with its polarizing axis. Both materials are homogenous.

2. **Formulation of the problem by using the theory of space curved beams**

The investigation follows the way as shown in [1]. Here, we simplify those equations, due to the fact that our structure has an initial planar form with constant initial radius of curvature. Furthermore, initially the cross-sections are not twisted. The geometrical arrangement is such that the so-called laminar piezoelectric effect dominates in the design, so the electric field in the η-direction causes expansion or contraction in the ζ-direction, which results in bending around the ξ-direction. Let us consider an arbitrary part of the beam with a width b and a thickness $2d + c$ as shown in Figure 2.

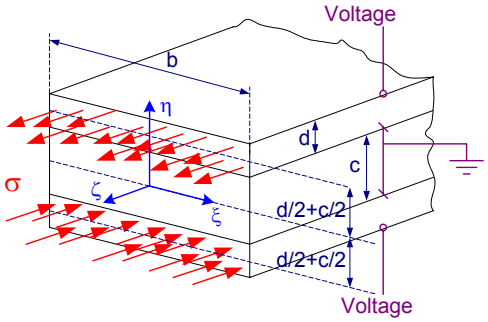

Figure 2. Tensile stresses in piezoelectric layers

The internal stress in a piezoelectric layer can be written as [2]

$$\sigma_{\varsigma pi} = E_{pi}\varepsilon_{\varsigma_0}\eta - e_{\eta\varsigma}E_\eta, \tag{2.1}$$

where $e_{\eta\varsigma}$ is the corresponding piezoelectric coefficient. The electric field E_η is known as the negativ gradient of the electric potential and is determined here as the difference ratio $-\frac{Voltage}{d}$. E_{pi} is the Young's modulus of the piezoelectric material. The strain

$\varepsilon_{\varsigma_0}$ on the centerline can be written in the form

$$\varepsilon_{\varsigma_0} = -\frac{1}{R^2}\frac{d^2v}{d\varphi^2} - \frac{1}{R}\gamma \tag{2.2}$$

which is a basic relation for the prismatic planar curvilinear beams with a constant radius of curvature R. Here, φ denotes the angle at center of the beam measured from the clamped end and is used as an independent variable. The variables v and γ represent the deflection of the beam in the η-direction and the twist of the beam, respectively.

There is a stress in the midlayer which can be calculated in the knowledge of the strain. By denoting the Young modulus of that layer by E_{Al}, we can write

$$\sigma_{\varsigma Al} = E_{Al}\varepsilon_{\varsigma_0}\eta. \tag{2.3}$$

Integrating $\sigma_{\varsigma pi}$ and $\sigma_{\varsigma Al}$ over the corresponding surfaces $A_{pi} = bd$ and $A_{Al} = bc$, respectively, we determine the global bending moment in the ξ-direction

$$M_\xi = \int\limits_{A_{pi}} \sigma_{\varsigma pi}\eta dA + \int\limits_{A_{Al}} \sigma_{\varsigma Al}\eta dA. \tag{2.4}$$

Performing the integrations in (2.4) and substituting (2.2), the moment can be expressed as

$$M_\xi = I_{\xi E}\left(-\frac{1}{R^2}\frac{d^2v}{d\varphi^2} - \frac{1}{R}\gamma\right) - 2e_{\eta\varsigma}E_\eta b\left(\frac{d}{2} + \frac{c}{2}\right), \tag{2.5}$$

where $I_{\xi E}$ is the bending rigidity of the cross-section. In a later section we wish to bring $I_{\xi E}$ into sharper focus. Similarly, the torsional mode is also taken into account and the torsional moment can be formulated as

$$M_\zeta = I_{cG}\left(\frac{1}{R}\frac{d\gamma}{d\varphi} - \frac{1}{R^2}\frac{dv}{d\varphi}\right), \tag{2.6}$$

where I_{cG} is the torsional rigidity of the-cross section.

3. Solution of the differential equation system

Since there are no external mechanical loads in our study, M_ξ and M_ζ are zero. Hence, (2.5) and (2.6) can be rearranged

$$I_{\xi E}\left(\frac{1}{R^2}\frac{d^2v}{d\varphi^2} + \frac{1}{R}\gamma\right) = -2e_{\eta\varsigma}E_\eta b\left(\frac{d}{2} + \frac{c}{2}\right), \tag{3.1a}$$

$$I_{cG}\left(\frac{1}{R}\frac{d\gamma}{d\varphi} - \frac{1}{R^2}\frac{dv}{d\varphi}\right) = 0\,. \tag{3.1b}$$

Equations (3.1a) and (3.1b) are coupled with the variables v and γ. We can eliminate the torsional rigidity in (3.1b) and by solving the differential equation

$$\frac{d\gamma}{d\varphi} - \frac{1}{R}\frac{dv}{d\varphi} = 0 \tag{3.2}$$

with the boundary conditions $v\,|_{\varphi=0} = 0$, $\gamma\,|_{\varphi=0} = 0$, we get the relation between the twist and the deflection of the beam as

$$\gamma = \frac{v}{R}. \tag{3.3}$$

Substituting (3.3) into (3.1a), an inhomogenous second order differential equation is obtained

$$\frac{d^2v}{d\varphi^2} + v = -2\frac{R^2}{I_{\xi E}} e_{\eta\varsigma} E_\eta b \left(\frac{d}{2} + \frac{c}{2}\right). \tag{3.4}$$

The solution is looked for in the form $v = A\cos\varphi + B\sin\varphi - 2\frac{R^2}{I_{\xi E}} e_{\eta\varsigma} E_\eta b \left(\frac{d}{2} + \frac{c}{2}\right)$, which is a sum of the general solution of the homogenous equation and of a particular solution. Here A and B are constants. The related boundary conditions are $v\,|_{\varphi=0} = 0$, $\frac{dv}{d\varphi}\,|_{\varphi=0} = 0$. The solution of the boundary value problem can be written in the form

$$v(\varphi) = 2\frac{R^2}{I_{\xi E}} e_{\eta\varsigma} E_\eta b \left(\frac{d}{2} + \frac{c}{2}\right)(\cos\varphi - 1)\,, \tag{3.5}$$

which is a trigonometric function of φ.

4. **Determining the bending rigidity of a composite beam**

Let us consider the symmetrical cross-section of the beam (Figure 3). The inertia of the extreme layers has the form

$$I_{\xi_{extr}} = b\left(\frac{d^3}{3} + \frac{d^2c}{2} + \frac{dc^2}{4}\right), \tag{4.1}$$

where b is the width of the cross-section, c means the thickness of the midlayer, d is the thickness of each extreme layer. The inertia of the midlayer can be written as

$$I_{\xi_{mid}} = \frac{bc^3}{12}. \tag{4.2}$$

To obtain the bending rigidity of the cross-section, (4.1) and (4.2) are coupled to each other through the Young's moduli of the midlayer E_{Al} and of the extreme layers E_{pi}, respectively

$$I_{\xi E} = 2I_{\xi_{extr}} E_{pi} + I_{\xi_{mid}} E_{Al}. \tag{4.3}$$

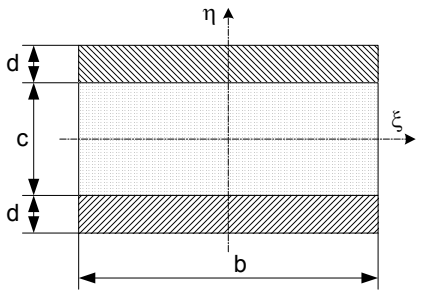

Figure 3. Cross-section of a 3-layered beam

If each layer has the same size, ie., their thicknesses are the same $\left(c = d = \frac{s}{3}\right)$ (Figure 1), then the expression of rigidity is reducible and has the form

$$I_{\xi E} = \frac{bs^3}{12}\left(\frac{26}{27}E_{pi} + \frac{1}{27}E_{Al}\right). \tag{4.4}$$

With the same consideration, (3.5) needs alteration. Substituting (4.4) into (3.5) and considering that $\left(\frac{d}{2} + \frac{c}{2}\right) = \frac{s}{3}$, we obtain the deflection of the neutral elastic fibre in the form

$$v(\varphi) = \frac{72R^2 e_{\eta\varsigma} E_\eta}{s\,(26E_{pi} + E_{Al})}(\cos\varphi - 1). \tag{4.5}$$

The twist of the beam obtained by substituting (4.5) into (3.3) has the form

$$\gamma(\varphi) = \frac{72Re_{\eta\varsigma} E_\eta}{s\,(26E_{pi} + E_{Al})}(\cos\varphi - 1). \tag{4.6}$$

Let us notice that the width of the beam b plays no role in the solution.

5. Solution of the problem by the FEM

The general form of the functional related to the problem is presented in [3]. In what follows we simplify it with respect to the quasi-static motion, hence D'Alambert's term is missing. Further no external mechanical loads are applied to the beam. All the electromechanical devices work as actuators, hence the electric potential is not varied, and the electric charge sources are omitted. The simplified functional can be expressed as

$$\int\limits_V \left(\delta\mathbf{u}^T \partial_{\mathbf{u}}^T\right) \mathbf{C}\left(\partial_{\mathbf{u}}\mathbf{u}\right) dV + \int\limits_V \left(\delta\mathbf{u}^T \partial_{\mathbf{u}}^T\right) \mathbf{e}\left(\partial_\Phi \Phi\right) dV = 0\,, \tag{5.1}$$

where $\mathbf{C}$ is the elasticity matrix, $\mathbf{e}$ is the piezoelectric matrix, $\mathbf{u}$ is the vector of the mechanical displacements and is chosen as the primary variable, Φ is the electric potential applied on the piezoelectric surfaces. The differential operators ∂_u, ∂_Φ generate the mechanical strains and electric fields, respectively. Superscript T denotes the transpose of objects. The mechanical displacements in an arbitrary element e are written in the form

$$\mathbf{u}^e\left(x, y, z\right) = \sum_n^p N_n^e\left(\overline{\xi}, \overline{\eta}, \overline{\zeta}\right) \mathbf{q}_n^e\,, \tag{5.2}$$

where N_n^e is the approximation fuction of the n-th node and $\mathbf{q}_n^e$ denotes the nodal displacement vector. The mapping between the local system $\left\{\overline{\xi}, \overline{\eta}, \overline{\zeta}\right\}$ and the global system $\{x, y, z\}$ is performed by using the blending functions [4] or the approximation functions. No confusion should arise if we define the local system by the coordinates $\overline{\xi}, \overline{\eta}, \overline{\zeta}$, because those are not identical with ξ, η, ζ presented in the previous sections. Although we can exactly describe the geometry of the elements in a parametric form, since their curvatures are given circular segments, or given straight line segments (Figure 4), the isoparametric mapping is also applied to control this technique.

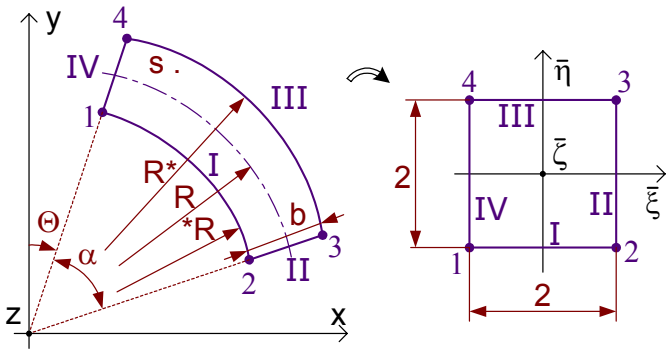

Figure 4. Mapping of an arbitrary circle-sided quadrilateral element

The coordinates x and y are obtained by

$$x = \frac{1-\overline{\eta}}{2} x_I\left(\overline{\xi}\right) + \frac{1+\overline{\eta}}{2} x_{III}\left(\overline{\xi}\right) \ , \tag{5.3a}$$

$$y = \frac{1-\overline{\eta}}{2} y_I\left(\overline{\xi}\right) + \frac{1+\overline{\eta}}{2} y_{III}\left(\overline{\xi}\right) \tag{5.3b}$$

with the functions associated with the edges I and III as

$$x_I\left(\overline{\xi}\right) = {}^*R \sin\left(\Theta + \frac{\alpha}{2} + \overline{\xi}\frac{\alpha}{2}\right) \ , \tag{5.4a}$$

$$x_{III}\left(\overline{\xi}\right) = R^* \sin\left(\Theta + \frac{\alpha}{2} + \overline{\xi}\frac{\alpha}{2}\right) \ , \tag{5.4b}$$

where ${}^*R$ and R^* are the radii of the inner and outer boundary curves, α is the angle at centre, Θ is the preangle, which is measured from zero to the IV^{th} edge. Taking the same geometry for each element (α) we write for the e-th element (as $e = 0, 1, 2, ..., m$), $\Theta = e\alpha$. From Figure 4 it is seen that the radius of the centerline R and the width of the element b are determined by the inner and outer radii as

$$R = \frac{{}^*R + R^*}{2} \ , \tag{5.5a}$$

$$b = \frac{R^* - {}^*R}{2} \ . \tag{5.5b}$$

Substituting (5.4a) and (5.4b) into (5.3a) and using (5.5a) and (5.5b) we get

$$x = \left(R + \overline{\eta}\frac{b}{2}\right) \sin\left[\frac{\alpha}{2}\left(2e + 1 + \overline{\xi}\right)\right] . \tag{5.6}$$

Similarly, the coordinate y can also be determined in the same manner, by using the corresponding blending functions belonging to the edges I and III as

$$y_I\left(\overline{\xi}\right) = {}^*R \cos\left(\Theta + \frac{\alpha}{2} + \overline{\xi}\frac{\alpha}{2}\right) , \tag{5.7a}$$

$$y_{III}\left(\overline{\xi}\right) = R^* \cos\left(\Theta + \frac{\alpha}{2} + \overline{\xi}\frac{\alpha}{2}\right) \tag{5.7b}$$

while y is obtained by substituting (5.7a) and (5.7b) into (5.3b) and has the form

$$y = \left(R + \overline{\eta}\frac{b}{2}\right)\cos\left[\frac{\alpha}{2}\left(2e + 1 + \overline{\xi}\right)\right] . \tag{5.8}$$

Since coordinates $\overline{\zeta}$ and z are independent of all $\overline{\xi}$, $\overline{\eta}$, x, y coordinates, the mapping between them is written as $z = \frac{s}{6}\overline{\zeta}$. The derivatives of approximation functions are said to be in the global system $\{x, y, z\}$, although $N_n^e\left(\overline{\xi}, \overline{\eta}, \overline{\zeta}\right)$ can be derived in the local $\left\{\overline{\xi}, \overline{\eta}, \overline{\zeta}\right\}$ system. Hence, the Jacobian matrix is introduced as

$$\mathbf{J}^e = \begin{bmatrix} \frac{\partial x}{\partial \overline{\xi}} & \frac{\partial y}{\partial \overline{\xi}} & \frac{\partial z}{\partial \overline{\xi}} \\ \frac{\partial x}{\partial \overline{\eta}} & \frac{\partial y}{\partial \overline{\eta}} & \frac{\partial z}{\partial \overline{\eta}} \\ \frac{\partial x}{\partial \overline{\zeta}} & \frac{\partial y}{\partial \overline{\zeta}} & \frac{\partial z}{\partial \overline{\zeta}} \end{bmatrix}^e = \begin{bmatrix} \frac{\alpha}{2}\left(R + \overline{\eta}\frac{b}{2}\right)\cos\alpha_e & -\frac{\alpha}{2}\left(R + \overline{\eta}\frac{b}{2}\right)\sin\alpha_e & 0 \\ \frac{b}{2}\sin\alpha_e & \frac{b}{2}\cos\alpha_e & 0 \\ 0 & 0 & \frac{s}{6} \end{bmatrix}, \tag{5.9}$$

where $\alpha_e = \frac{\alpha}{2}\left(2e + 1 + \overline{\xi}\right)$. The mapping is not degenerate if the inverse mapping exists. A necessary condition for this is that the determinant of the Jacobian matrix is positive. This criterium is satisfied if $R > \frac{b}{2}$.

In this paper the well known polynomial approximation of the geometry is also applied. The curved sides (I and III) of the element are written with the same Legendre polynomials which are used to approximate the mechanical displacement. This is the technique of the isoparametric mapping and detailed in the literature [5].

A p-extensional computational technique allows us to estimate the exact elasticity solution and the relative error [5]. The error $\|e\|_{(p)}$ is estimated on a nonrefined mesh as

$$\|e\|_{(p)} \leq kN_{(p)}^{-\beta}, \tag{5.10}$$

where p is the order of the approximation, $N_{(p)}$ is the number of unknowns, k and β are positive constants. By defining the estimated error difference at (p), $(p-1)$, $(p-2)$, β can be eliminated

$$\lg\|e\|_{(p)} - \lg\|e\|_{(p-1)} = -\beta(\lg N_{(p)} - \lg N_{(p-1)}), \tag{5.11a}$$

$$\lg\|e\|_{(p-1)} - \lg\|e\|_{(p-2)} = -\beta(\lg N_{(p-1)} - \lg N_{(p-2)}). \tag{5.11b}$$

By introducing the exponent

$$Q = \frac{\lg\left(\frac{N_{(p-1)}}{N_{(p)}}\right)}{\lg\left(\frac{N_{(p-2)}}{N_{(p-1)}}\right)} \tag{5.12}$$

we rewrite (5.11a) and (5.11b) in the form

$$\lg\left(\frac{\|e\|_{(p)}}{\|e\|_{(p-1)}}\right) = \lg\left(\frac{\|e\|_{(p-1)}}{\|e\|_{(p-2)}}\right)^Q . \tag{5.13}$$

By using the relationship between the energy norms of the exact elasticity solution $\|u\|$ and of the FEM-approximated solution at a given polynomial degree $\|u_{FEM}\|_{(p)}$

the error can be expressed as

$$\|e\|^2_{(p)} = \|u\|^2 - \|u_{FEM}\|^2_{(p)}. \tag{5.14}$$

Introducing (5.14) into (5.13) we get

$$\frac{\|u\|^2 - \|u_{FEM}\|^2_{(p)}}{\|u\|^2 - \|u_{FEM}\|^2_{(p-1)}} = \left(\frac{\|u\|^2 - \|u_{FEM}\|^2_{(p-1)}}{\|u\|^2 - \|u_{FEM}\|^2_{(p-2)}} \right)^Q, \tag{5.15}$$

which makes it possible to determine the norm of the exact elasticity solution $\|u\|$ and of the real error $\|e\|_{(p)}$ by using (5.14) again.

6. **Numerical example**

Figure 1 illustrates the structure under investigation. Each layer has the thickness of $\frac{s}{3} = 1\ mm$, the radius of the curvature of the beam is $R = 60\ mm$, the width of the beam is $b = 8\ mm$. The angle at the center of the whole domain is 180°. The structure is built up by using 3D higher-order solid elements. Figure 5 shows the table with the unknown parameters as a functions of the polynomial order and the angle at the center of the element. The number of elements is 18 ($\alpha = 30°$), 27 ($\alpha = 20°$) and 54 ($\alpha = 10°$).

p	α = 30deg	α = 20deg	α = 10deg
2	522	756	1458
3	876	1272	2460
4	1473	2148	4173
5	2313	3384	6597
6	3450	5061	9894
7	4938	7260	14226
8	6831	10062	19755

Figure 5. Table of the number of the unknown parameters in each case of meshing

For approximation Legendre polynomials are used from the classical truncated space, for numerical integration 10 Gaussian points are chosen in all directions of the 3D space. Besides the blending function method the traditional isoparametric mapping is performed with the same number of approximation functions as used in the displacement approximation and the results are compared in this regard also. Both piezoelectric actuators are supplied with the constant electric potential of DC 100 Voltage and the deformation of the beam consists of two forms. First, it deflects, second, its cross-sections rotate. Figure 6 shows the displacements in a direction perpendicular to the $\{\xi, \zeta\}$ plane vs. φ. In Figure 7 the twist of the beam is plotted vs. φ. Solid lines belong to linear beam theory, dashed lines to FEM result at p=8. ($\alpha = 10°$). The results agree well. Relative discrepancies between analytical and FEM results at $\varphi = 180°$ are less than 0.1 %.

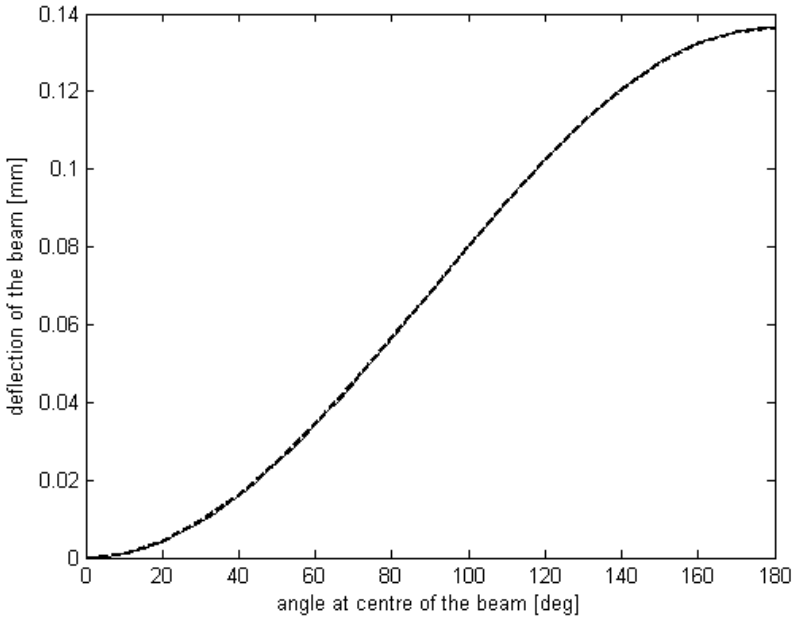

Figure 6. Bending of the beam along the centerline

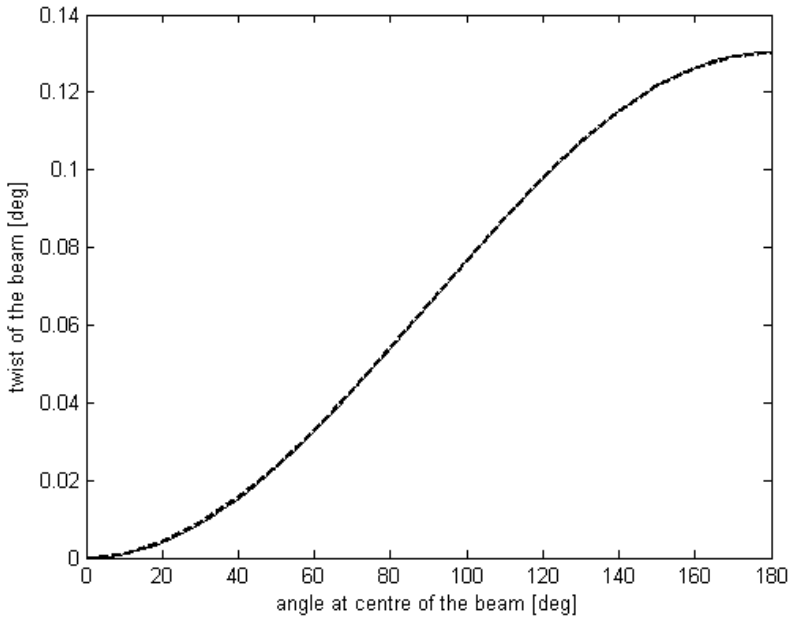

Figure 7. Rotation of the cross-sections along the centerline

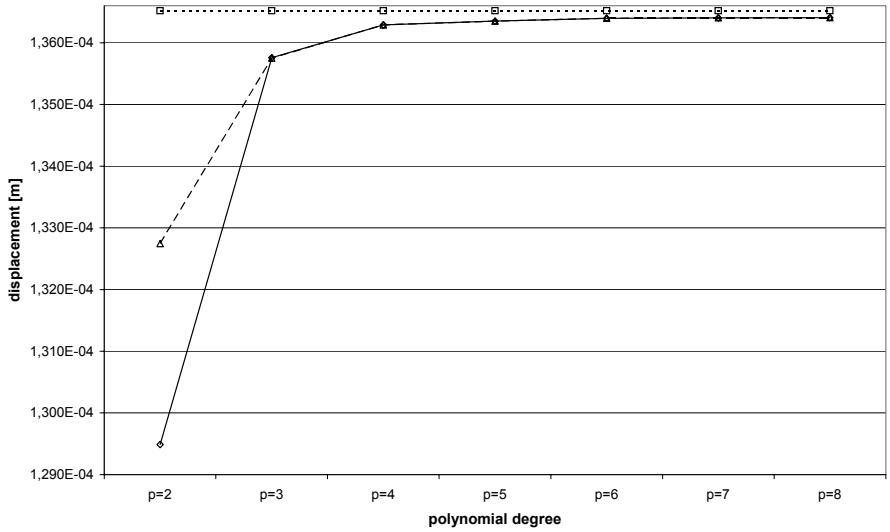

Figure 8a. Displacement of the last cross-section vs. polynomial degree at $\alpha = 30°$

Displacement in the η-direction of the last cross-section is computed for different mesh and mapping. Figures 8a,b and c depict the results. Dotted lines show the beam-theory result. Dashed lines belong to the FEM isoparametric mapping, solid lines stand for the FEM blending function mapping.

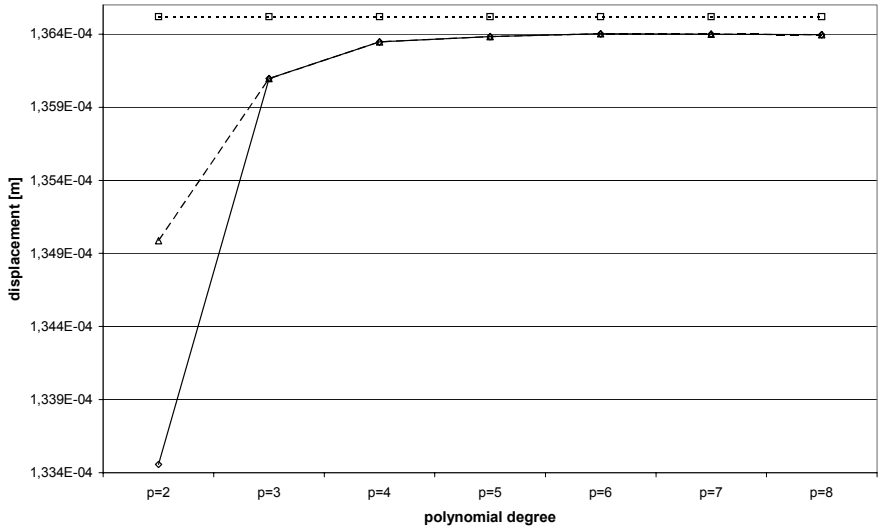

Figure 8b. Displacement of the last cross-section vs. polynomial degree at $\alpha = 20°$

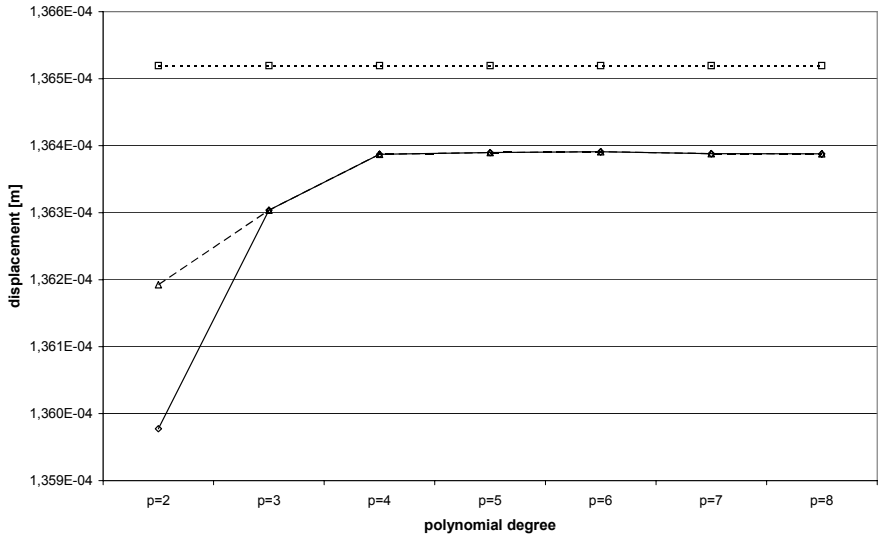

Figure 8c. Displacement of the last cross-section vs. polynomial degree at $\alpha = 10°$

Figure 9 illustrates the convergence of the solution. The strain energy norm vs. order of the polynomial approximation at $\alpha = 30°$, $20°$ and $10°$ and with two different geometry mapping is drawn with dotted, dashed and solid lines, respectively. The strain energy norm of the exact elasticity solution is drawn with dashdot line.

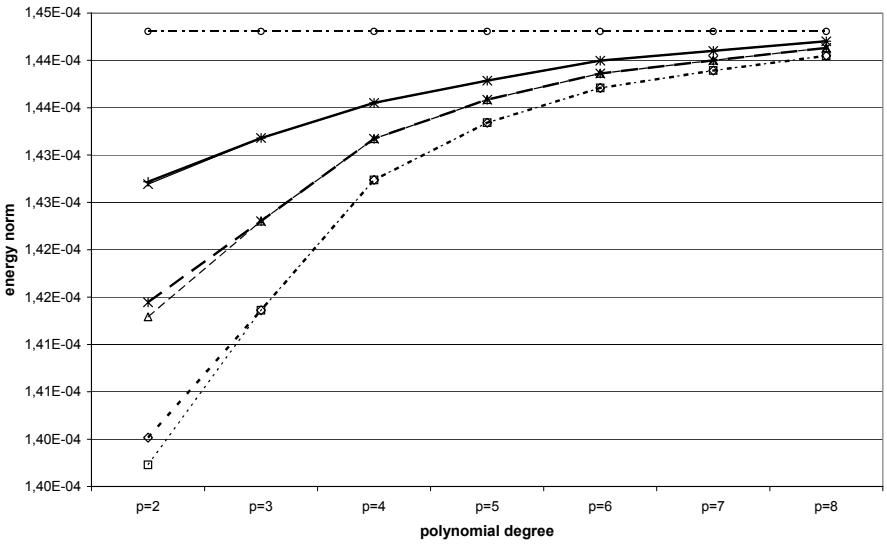

Figure 9. Strain energy norm at $\alpha = 30°$, $20°$, $10°$

It can be clearly seen that the difference between the results of the blending function method and isoparametric mapping is not significant at a higher polynomial degree. The sharp discrepancy in the displacement values arises only at $p = 2$. The relative error in energy norm is also presented for uniform $p = 2, 3, 4, 5, 6, 7, 8$ distribution. Since there is no significant difference in energy norm at $p = 6, 7, 8$ between the two types of mapping, the error estimation is performed by using the values computed with the isoparametric mapping. In Figure 10a, b, c in semilog scale the error decreases in each case ($\alpha = 30°$, $20°$, $10°$), from which it follows that the convergence is exponential.

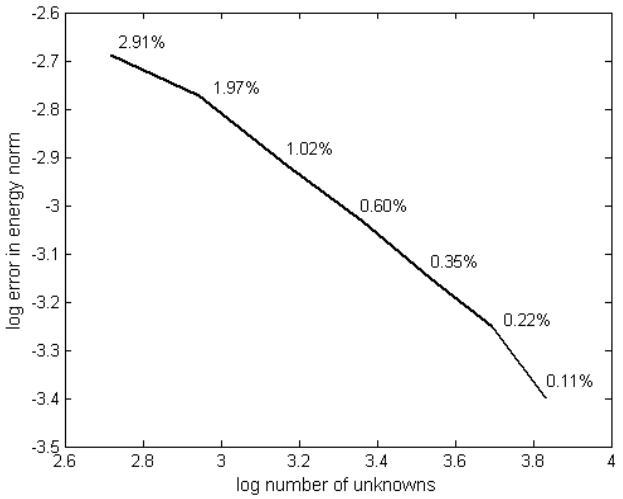

Figure 10a. Error of uniform p-distribution on nonrefined mesh ($\alpha = 30°$)

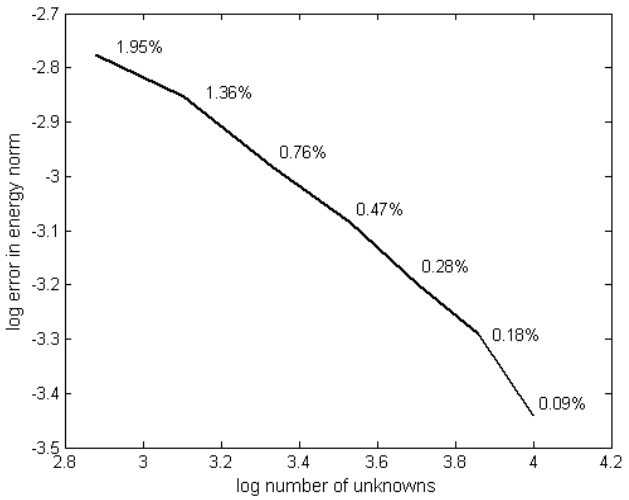

Figure 10b. Error of uniform p-distribution on nonrefined mesh ($\alpha = 20°$)

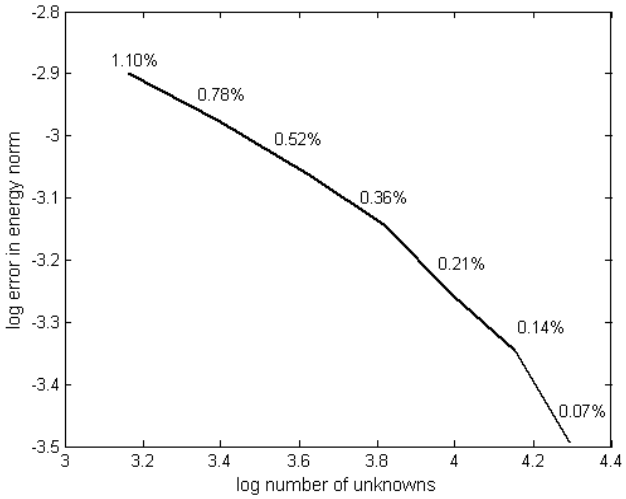

Figure 10c. Error of uniform p-distribution on nonrefined mesh ($\alpha = 10°$)

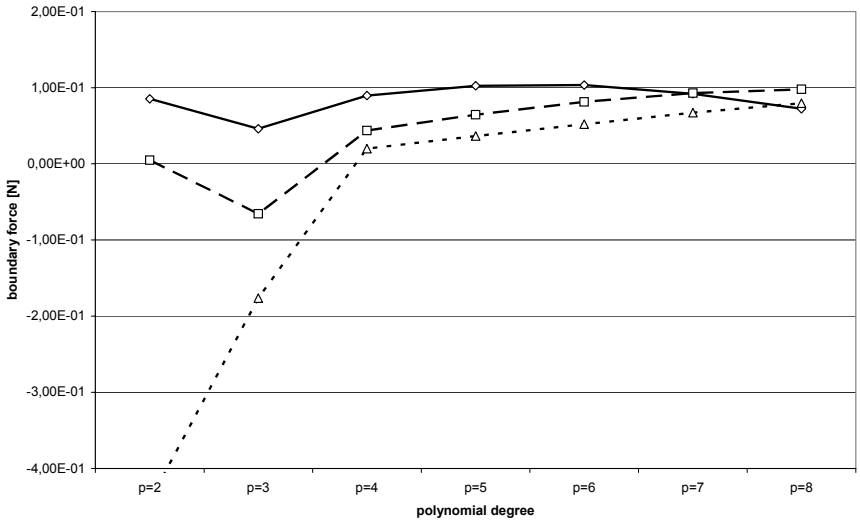

Figure 11a. Dynamic boundary condition (η-force of the last cross section) computed with the blending function method

The satisfaction of the dynamic boundary condition is also investigated. The force on the last cross-section in the η-direction is the most important variable here. This is computed for uniform $p = 2, 3, 4, 5, 6, 7, 8$ distribution in three different meshes ($\alpha = 30°$, $20°$, $10°$) and with two mapping techniques. Figure 11a illustrates the force for blending function mapping and Figure 11b for isoparametric mapping.

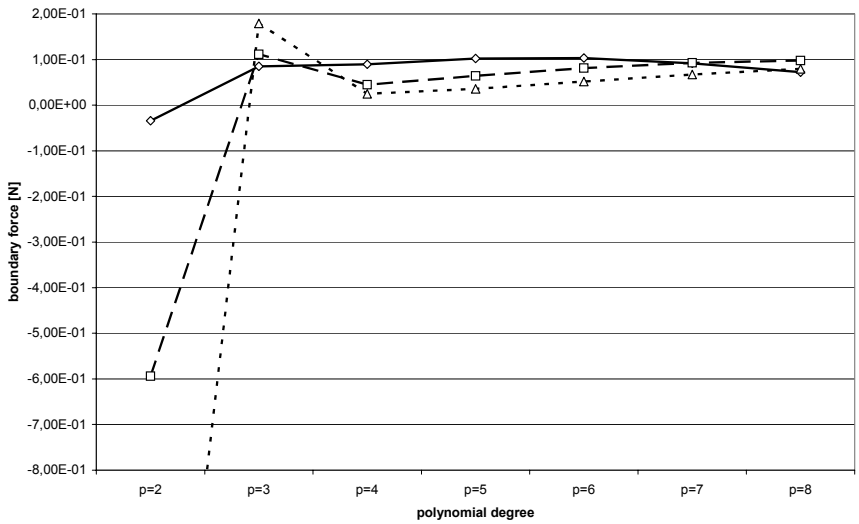

Figure 11b. Dynamic boundary condition (η-force of the last cross section) computed with isoparametric mapping

In both diagrams the dotted line belongs to $\alpha = 30°$, the dashed line to $\alpha = 20°$, and the solid line to $\alpha = 10°$. The diagram shows that at $p = 2, 3$ values the results oscillate. If $p = 4, 5, 6$ the force gets a little value, which is about $0.1N$, although at higher p values the results decrease and tend to zero. The procedure is fast if the mesh is smooth and slow with large elements. For example at $p = 8$ if $\alpha = 30°$ the force tends to its maximum, if $\alpha = 20°$, it has already reached the maximum, and if $\alpha = 10°$, the descent can be clearly seen.

7. **Conclusions and remarks**

In this paper the deformation of a multilayered piezoelectric semiring was presented. An electric field was applied in PZT patches bonded to the semicircular planar prismatic beam, which resulted in the deflection of the beam as it was expected and additionally in the rotation of its cross-sections. These deformations were determined analytically by using the linear theory of 3D curved beams and compared to the approximate solution obtained by the use of FEM. Solid p-extensional elements were used, due to the fact that the problem was non-symmetrical 3D. At 2, 3, 4, 5, 6, 7, 8 polynomial degrees of approximations the relative error was computed, which justifies the convergence of the numerical solution. It was presented that both the deflection and the twist of the beam were cosine functions of the angle of the arc of the centerline. It was also shown that the radius of curvature plays an important role, since it creates a proportional relationship between the deflection and the twist of the beam, but the width of the beam does not influence the result. Following this train of thought further conclusions can be drawn. Comparing the theoretical solution, which was a simple 1D case (ie. $e_{\eta\varsigma}$, E_{pi}), with the 3D FEM solution the bending around

direction η is not significant, since it was neglected in the analytical solution but FEM added the energy of this mode to the other ones. It is remarkable that the change of thickness of piezoelectric layers can be also negligible in thin patches. These discrepancies cause the differences between theoretical and FEM solutions. Comparing the two mapping techniques, it is clearly seen that in lower p-distribution the blending function method gave less adequate results than the isoparametric mapping but in higher modes both techniques are equally applied, because the rigid-body rotations tend to zero [4].

Acknowledgement. This work has been supported by grant OTKA Hungarian Fund for Scientific Research No. T030096, the Hungarian Ministry of Education No. FKFP 0504/2000. The support is gratefully acknowledged.

REFERENCES

1. Ponomarjov, S. D.: *Calculus of Strength in Mechanical Engineering, Vol. 7*, Műszaki Könyvkiadó Budapest, 1966, 89-109. (in Hungarian)
2. Preumont, A.: *Vibration Control of Active Structures*, Kluwer Academic Publishers, 1997.
3. Berger, H., Cao, X., Köppe, H. and Gabbert, U.: *Finite element based analysis of adaptive structures*, Proc. of the Euromech 373 Colloquium: Modelling and Control of Adaptive Mechanical Structures, (1998), 73-81.
4. Szabó, B. and Babuska I.: *Finite Element Analysis*, John Wiley & Sons Inc., 1991, 107-112, 97-99, 239-241.
5. Paczelt, I.: *Finite Element Method in Engineering Practice, Vol. 1*, University Press, Miskolc, 1999, 421-445. (in Hungarian)

APPENDIX

3D piezoelectric matrix (PIC151):

$$\mathbf{e}^T = \begin{bmatrix} 0 & 0 & 0 & 0 & 0 & 12 \\ 0 & 0 & 0 & 0 & 12 & 0 \\ -9.6 & -9.6 & 15.1 & 0 & 0 & 0 \end{bmatrix} Cm^{-2}.$$

The 1D $e_{\eta\varsigma}$ piezoelectric coefficient is $-12.75\ Cm^{-2}$. The 3D piezoelectric elasticity matrix:

$$\mathbf{C}_{pi} = \begin{bmatrix} 10.76 & 6.312 & 6.385 & 0 & 0 & 0 \\ 6.312 & 10.76 & 6.385 & 0 & 0 & 0 \\ 6.385 & 6.385 & 10.04 & 0 & 0 & 0 \\ 0 & 0 & 0 & 1.962 & 0 & 0 \\ 0 & 0 & 0 & 0 & 1.962 & 0 \\ 0 & 0 & 0 & 0 & 0 & 2.224 \end{bmatrix} \times 10^{10} Nm^{-2}.$$

The Young modulus in 1D is $E_{pi} = 5.943 \times 10^{10}\, Nm^{-2}$. The isotropic aluminium material has a Young's modulus $E_{Al} = 6.865 \times 10^{10}\, Nm^{-2}$ and Poisson's ratio: $\nu = 0.34$.